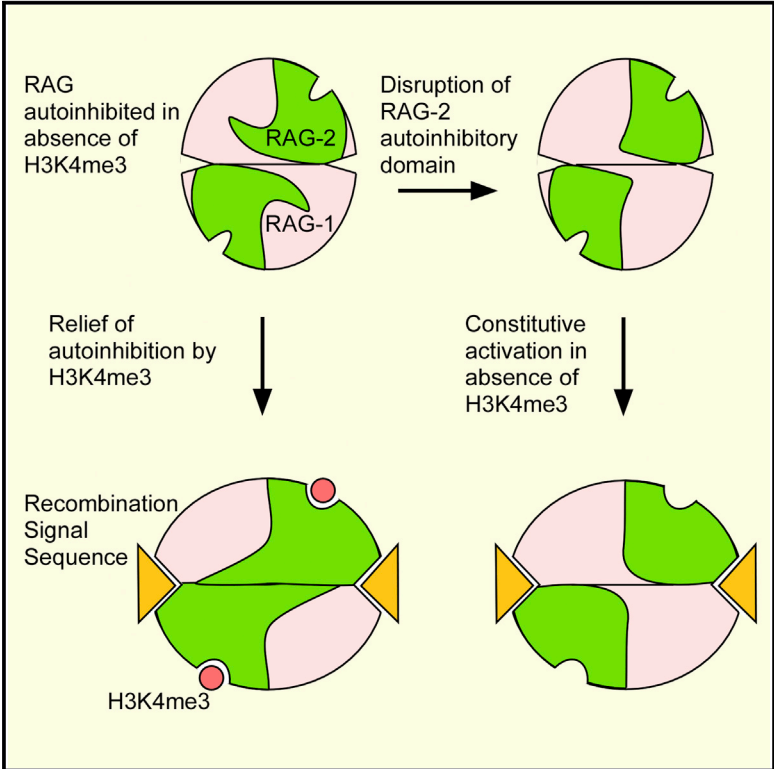# Cell Reports

An Autoregulatory Mechanism Imposes Allosteric Control on the V(D)J Recombinase by Histone H3 Methylation

Graphical Abstract

Authors

Chao Lu, Alyssa Ward, ..., Yun Liu, Stephen Desiderio

Correspondence

sdesider@jhmi.edu

In Brief

RAG initiates V(D)J recombination and is targeted to active chromatin. This coupling involves an interaction between RAG and H3K4me3. Lu et al. now identify an autoinhibitory domain within RAG whose disruption uncouples recombination from recognition of H3K4me3. This autoinhibitory mechanism enforces allosteric stimulation of RAG by active chromatin.

Highlights

- V(D)J recombination is stimulated by binding of H3K4me3 to RAG-2

- An autoinhibitory domain in RAG-2 confers responsiveness to H3K4me3

- Disruption of this domain mimics stimulation of wild-type RAG by H3K4me3

- Active chromatin allosterically stimulates RAG through relief of autoinhibition

CrossMark

CellPress

Report

An Autoregulatory Mechanism Imposes Allosteric Control on the V(D)J Recombinase by Histone H3 Methylation

Chao Lu,[1,2] Alyssa Ward,[1] John Bettridge,[1] Yun Liu,[1,3] and Stephen Desiderio[1,*]

[1]Department of Molecular Biology and Genetics and Institute for Cell Engineering, The Johns Hopkins University School of Medicine, Baltimore, MD 21205, USA
[2]Department of Physiology and Pathophysiology, School of Basic Medical Sciences, Fudan University, Shanghai 200032, China
[3]Present address: Center for Epigenetics, Institute for Basic Biomedical Sciences, The Johns Hopkins University School of Medicine, Baltimore, MD 21205, USA
*Correspondence: sdesider@jhmi.edu
 http://dx.doi.org/10.1016/j.celrep.2014.12.001

SUMMARY

V(D)J recombination is initiated by a specialized transposase consisting of the subunits RAG-1 and RAG-2. The susceptibility of gene segments to DNA cleavage by the V(D)J recombinase is correlated with epigenetic modifications characteristic of active chromatin, including trimethylation of histone H3 on lysine 4 (H3K4me3). Engagement of H3K4me3 by a plant homeodomain (PHD) in RAG-2 promotes recombination in vivo and stimulates DNA cleavage by RAG in vitro. We now show that H3K4me3 acts allosterically at the PHD finger to relieve autoinhibition imposed by a separate domain within RAG-2. Disruption of this autoinhibitory domain was associated with constitutive increases in recombination frequency, DNA cleavage activity, substrate binding affinity, and catalytic rate, thus mimicking the stimulatory effects of H3K4me3. Our observations support a model in which allosteric control of RAG is enforced by an autoinhibitory domain whose action is relieved by engagement of active chromatin.
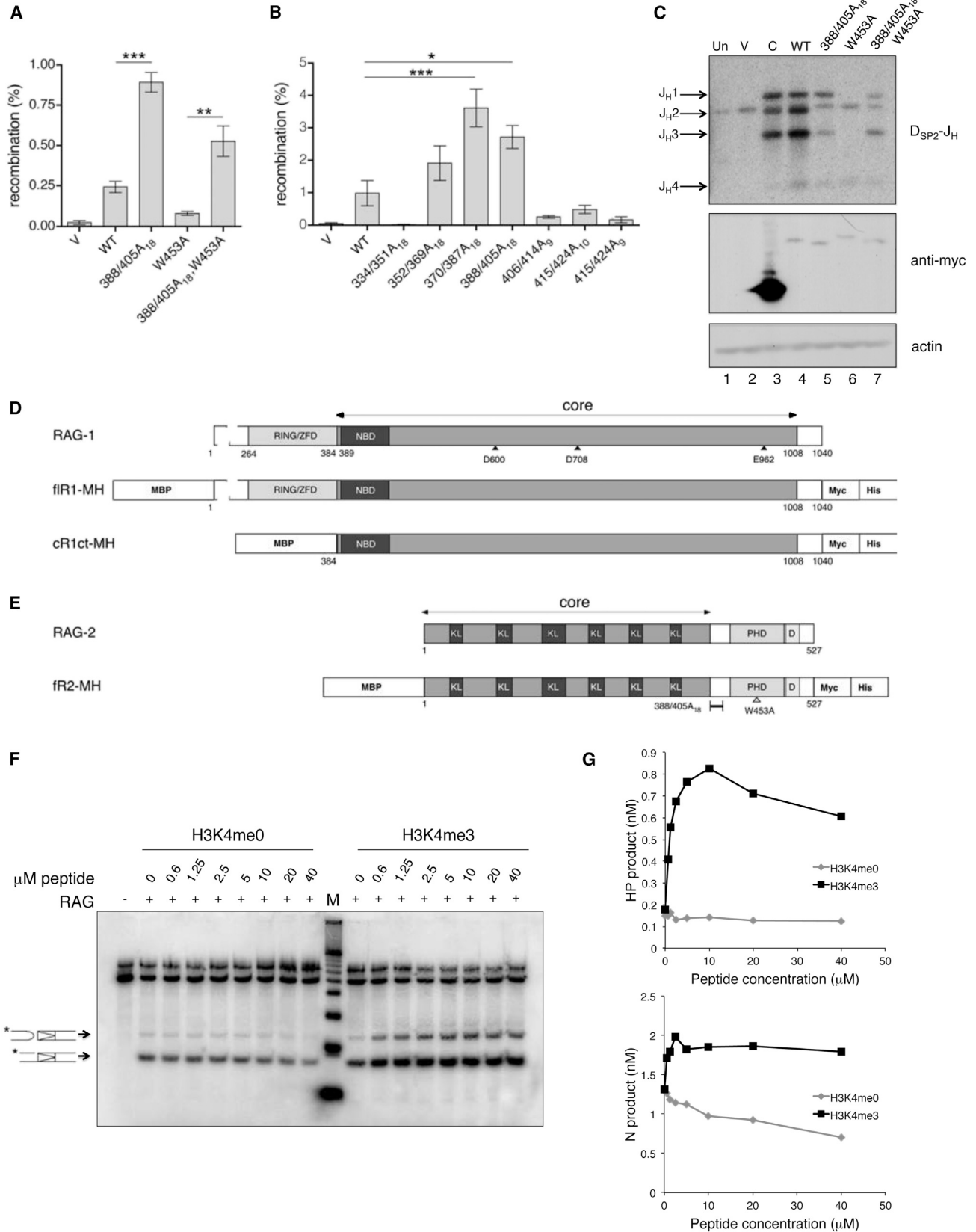
INTRODUCTION

During lymphocyte development, the genes encoding antigen receptors are assembled from discrete gene segments by V(D)J recombination. This process is initiated by the proteins RAG-1 and RAG-2, which together cleave DNA at recombination signal sequences (RSSs) that flank the participating gene segments (Gellert, 2002; Schatz and Swanson, 2011). There are two classes of RSSs, termed 12-RSS and 23-RSS, in which heptamer and nonamer elements are separated by spacers of 12 bp or 23 bp, respectively. DNA cleavage by RAG involves nicking at the junction between the RSS and the coding sequence, followed by transesterification to produce a blunt, 5′-phosphorylated signal end and a coding end that terminates in a hairpin. Under physiologic conditions, cleavage requires the pairing of a 12-RSS with a 23-RSS, so that recombination between like segments is suppressed (Schatz and Swanson, 2011).

V(D)J recombination acts in an ordered, locus-specific fashion during lymphoid development. In the B lineage, for example, the immunoglobulin heavy chain (IgH) locus is rearranged before the light chain loci and assembly of an immunoglobulin heavy chain gene proceeds by sequential D-to-J_H and V_H-to-DJ_H joining (Alt et al., 1984). Productive rearrangement suppresses further recombination at the IgH locus, thereby enforcing monoallelic expression of immunoglobulin heavy chain (Jung et al., 2006). The ability of gene segments to undergo V(D)J recombination is positively correlated with histone modifications characteristic of active chromatin, including hypermethylation of histone H3 at lysine 4 (Chakraborty et al., 2007; Goldmit et al., 2005; Liu et al., 2007; Matthews et al., 2007; Morshead et al., 2003; Subrahmanyam et al., 2012).

RAG-1 and RAG-2 are 1,040 and 527 amino acid residues long, respectively. Although the canonical noncore region of RAG-2, comprising residues 387 through 527, is dispensable for DNA cleavage in vitro, removal of this region is associated with decreased recombination frequency (Steen et al., 1999) and increased aberrant recombination in vivo (Sekiguchi et al., 2001; Talukder et al., 2004). Interpretation of these effects is complicated by the presence of domains within the RAG-2 noncore region that support destruction at the G1-S transition (Jiang et al., 2005; Lee and Desiderio, 1999; Li et al., 1996; Zhang et al., 2011), nuclear import (Ross et al., 2003), and binding to H3K4me3 (Liu et al., 2007; Matthews et al., 2007; Ramón-Maiques et al., 2007). This last function is served by a plant homeodomain (PHD) finger spanning residues 415 through 487 (Callebaut and Mornon, 1998; Ramón-Maiques et al., 2007). Binding of H3K4me3 by the PHD finger promotes recombination in vivo (Liu et al., 2007; Matthews et al., 2007) and H3K4me3-bearing peptides stimulate DNA cleavage by RAG in vitro (Grundy et al., 2010; Shimazaki et al., 2009), suggesting that H3K4me3 is an allosteric activator of the V(D)J recombinase.

Paradoxically, removal of the RAG-2 noncore region impairs V(D)J recombination less severely than does selective mutation of the PHD finger (Cuomo and Oettinger, 1994; Sadofsky et al., 1994). Moreover, core RAG-2 supports D-to-J_H joining in vivo

A

B

C

Un V C WT 388/405A₁₈ W453A 388/405A₁₈, W453A

J_H1 →
J_H2 →
J_H3 →

J_H4 →

D_{SP2}-J_H

anti-myc

actin

1 2 3 4 5 6 7

D

core

RAG-1

1   264   RING/ZFD   384 389   NBD   D600   D708   E962   1008   1040

flR1-MH

MBP   1   RING/ZFD   NBD   1008 1040   Myc   His

cR1ct-MH

MBP   384   NBD   1008 1040   Myc   His

E

core

RAG-2

1   KL KL KL KL KL KL   PHD   D   527

fR2-MH

MBP   1   KL KL KL KL KL KL   PHD   D   Myc   His
388/405A₁₈   W453A   527

F

H3K4me0   H3K4me3

µM peptide   0 0.6 1.25 2.5 5 10 20 40   M   0 0.6 1.25 2.5 5 10 20 40
RAG   - + + + + + + + +   + + + + + + + +

G

HP product (nM)

H3K4me0
H3K4me3

Peptide concentration (µM)

N product (nM)

H3K4me0
H3K4me3

Peptide concentration (µM)

(legend on next page)

([Akamatsu et al., 2003; Kirch et al., 1998; Liang et al., 2002](#)), while the full-length RAG-2(W453A) mutant, which is unable to bind H3K4me3, does so only weakly ([Liu et al., 2007](#)). These observations suggested the presence within RAG-2 of an autoinhibitory domain that is absent from the core fragment. We now uncover an autoregulatory region within RAG-2 that imposes allosteric control on V(D)J recombination. Disruption of autoinhibition mimics engagement of H3K4me3. Our observations support a model in which epigenetic control of RAG is enforced by an auto-inhibitory domain whose action is relieved by active chromatin.

RESULTS

Identification of an Autoinhibitory Domain within the RAG-2 Noncore Region

We reasoned that an autoinhibitory domain would be identifiable by second site mutations that rescue the activity of RAG-2(W453A). Therefore, we scanned the entire canonical noncore region of RAG-2(W453A) with clustered alanine substitutions of nine or ten amino acid residues each. In a preliminary screen two contiguous secondary mutations, $388/396A_9$ and $397/405A_9$, rescued RAG-2(W435A) in an assay for V(D)J recombination (data not shown). Therefore, we constructed RAG-2 mutants bearing a clustered alanine substitution spanning residues 388 through 405 alone [RAG-2($388/405A_{18}$)] or in the presence of W453A [RAG-2($388/405A_{18}$, W453A)] ([Figure S1](#)A). The activity of RAG-2(W453A) in an assay for signal joining was impaired relative to wild-type, as reported previously ([Liu et al., 2007](#)). In contrast, the RAG-2($388/405A_{18}$, W453A) double mutant exhibited no such reduction ([Figure 1](#)A). Moreover, the RAG-2($388/405A_{18}$) single mutant was significantly more active than wild-type ([Figure 1](#)A). Differences in protein accumulation did not account for the effects of the $388/405A_{18}$ and W453A mutations ([Figure S1](#)B). The gain of function associated with the $388/405A_{18}$ mutation was consistently observed in separate assays for signal joining ([Figures 1](#)A, 1B, [S1](#)D, and S1E), in an assay for coding joining ([Figure S1](#)F), and in combination with a muta-

tion (T490A) that uncouples RAG-2 accumulation from the cell cycle ([Figure S1](#)G), suggesting that stimulation is independent of cell-cycle-dependent control. The $388/405A_{18}$ mutation had no apparent effect on the precision of signal joining ([Figures S1](#)H and S1I).

To define the amino-terminal boundary of the autoinhibitory domain we extended alanine scanning mutagenesis into the canonical core region of RAG-2 ([Figure S1](#)A). RAG-2($370/387A_{18}$) exhibited a gain-of-function phenotype similar to that of RAG-2($388/405A_{18}$), whereas RAG-2($352/369A_{18}$) was similar to wild-type and RAG-2($334/351A_{18}$) did not support recombination ([Figure 1](#)B). Mutations carboxy-terminal to residue 405 failed to confer a gain of function ([Figure 1](#)B). The $370/387A_{18}$ mutation was not associated with increased accumulation of RAG-2 ([Figure S1](#)C). These results are consistent with the presence of an autoinhibitory domain between amino acid residues 370 and 405 of RAG-2. The stimulatory effects of the $370/387A_{18}$ and $388/405A_{18}$ mutations were similar, and we performed subsequent assays with the latter.

Disruption of Autoinhibition Uncouples Recombination of Endogenous Gene Segments from H3K4me3 Recognition

We employed a qualitative assay to determine whether disruption of the putative RAG-2 autoinhibitory domain could bypass the dependence of endogenous D-to-J_H joining on H3K4me3 recognition. To do so, we expressed wild-type RAG-2, RAG-2($388/405A_{18}$), RAG-2(W453A), or RAG-2($388/405A_{18}$, W453A) in a RAG-2-deficient pro-B cell line using a retroviral vector that confers puromycin resistance. At 25 days of selection, DSP2-to-J_H joining was assayed ([Liu et al., 2007](#)). Rearrangements were detected in cells transduced with core RAG-2, wild-type RAG-2, or RAG-2($388/405A_{18}$) ([Figure 1](#)C, lanes 3–5). Rearrangements were profoundly reduced in cells transduced with RAG-2(W453A) ([Figure 1](#)C, lane 6). The debilitating effect of the W453A mutation was reversed, however, by mutation of residues 388–405 ([Figure 1](#)C, lane 7), consistent with the

Figure 1. Autoinhibition of RAG In Vivo and Stimulation of Chromatin-Depleted RAG by H3K4me3 In Vitro

(A) Rescue of an inactivating PHD finger mutation. Recombination (%), frequency of signal joining in cells transfected with pJH200 ([Hesse et al., 1987](#)), full-length RAG-1 and vector (V), full-length wild-type RAG-2 (WT), or full-length RAG-2 mutants as indicated (mean ± SEM, n = 3 independent biological replicates, representing ≥500 ampicillin (A)-resistant colonies per RAG-2 variant and ≥200 A-resistant colonies for vector alone). Significant differences were determined by ANOVA (***p < 0.001; **p < 0.01).

(B) Mapping of the autoinhibitory domain. Signal joining (mean ± SEM, n = 3 independent biological replicates, representing ≥100 A-resistant colonies per RAG-2 variant) was assayed using full-length RAG constructs and analyzed as in (A); ***p < 0.001; *p < 0.05.

(C) Rescue of W453A by $388/405A_{18}$ in an assay for endogenous recombination. Top: assay for D_{SP2}-to-J_H joints in genomic DNA from uninfected cells (Un) or cells transduced with the following: vector alone (V), core RAG-2 (C), full-length wild-type RAG-2 (WT), or full-length RAG-2 mutants. Positions of D_{SP2}-to-J_H recombinants are indicated at left. Middle and bottom: detection of myc-tagged RAG-2 species and actin, respectively, by immunoblotting.

(D) Diagrams of wild-type RAG-1 (top), full-length RAG-1-MH (flR1-MH, middle), and core RAG-1ct-MH (cR1ct-MH, bottom). Amino acid residues at domain boundaries are numbered. The core is designated in dark gray. The RING-type zinc-finger domain (RING/ZFD) and the nonamer binding domain (NBD) are indicated. Arrowheads, catalytic residues. MBP, Myc, and His denote the maltose binding protein, c-*myc* epitope, and polyhistidine tags, respectively.

(E) RAG-2 constructs for in vitro assays. Above: wild-type RAG-2. Below: full-length RAG-2 fusion protein. Amino acid residues at domain boundaries are numbered. The core is shown in dark gray. Kelch-like domains (KL), the PHD finger (PHD), and the degradation signal (D) are indicated. MBP, Myc, and His are as defined in (D). Positions of mutations are marked below.

(F) Stimulation of H3K4me3-depleted RAG by exogenous H3K4me3. Coupled cleavage reactions contained radiolabeled 12-RSS and unlabeled 23-RSS. Additions of RAG and H3K4me0 or H3K4me3 are indicated above. Positions of hairpin (HP) and nicked (N) products are indicated by arrows. M, 10 bp marker ladder. Uncleaved substrate migrates as a doublet, likely as a result of incompletely melted secondary structure.

(G) Accumulation of hairpin product (top) or nicked intermediates (bottom) at 1 hr is plotted in nM as a function of H3K4me0 (gray diamonds) or H3K4me3 (black squares) concentration.

Data in (F) and (G) are representative of more than three experiments.

interpretation that relief of autoinhibition bypasses the dependence of endogenous V(D)J recombination on recognition of H3K4me3 by RAG-2. Similar results were observed in two additional, independent transduction experiments (Figures S1J and S1K).

Robust Stimulation of RAG Activity by Exogenous H3K4me3 upon Removal of Endogenous H3K4me3

Although exogenous H3K4me3 has been shown to stimulate DNA cleavage by RAG, the responsiveness of standard RAG preparations has been inconsistent, suggesting variable contamination with endogenous H3K4me3. Indeed, standard amylose affinity preparations of MBP-tagged RAG fusion proteins (Figures 1D and 1E) contained H3K4me3 (Figure S2A, lanes 7 and 8). When we performed sonication before amylose affinity chromatography (Raval et al., 2008), contaminating H3K4me3 was removed (Figure S2A, lanes 1–3). All RAG preparations employed hereafter were depleted of endogenous H3K4me3 in this way.

We assessed the effect of exogenous H3K4me3 on DNA cleavage by RAG in the absence of endogenous H3K4me3. Here we employed a version of RAG-1 lacking the amino-terminal noncore region but retaining the carboxy-terminal noncore region (cR1ct-MH; Figure 1D) because RAG complexes containing cR1ct-MH are more robustly stimulated by H3K4me3 than complexes containing canonical core RAG-1 (Grundy et al., 2010) and because we obtained complexes containing cR1ct-MH in at least 20-fold-greater yield than complexes containing full-length RAG-1. Full-length RAG-2 (fR2-MH; Figure 1E) and cR1ct-MH fusion proteins were coexpressed and copurified (Figure S2B) free of detectable endogenous H3K4me3 (Figure S2A, lanes 4–6). This RAG complex was assayed for coupled cleavage of a radiolabeled 12-RSS substrate in the presence of unlabeled 23-RSS substrate and increasing amounts of a histone H3-derived peptide containing trimethylated lysine 4 (H3K4me3) or unmethylated lysine 4 (H3K4me0). Accumulation of nicked and hairpin products was stimulated in a dose-dependent fashion by H3K4me3, but not by H3K4me0 (Figures 1F and 1G, top). The yield of hairpin-end products showed about 4.5-fold maximal stimulation with half-maximal stimulation occurring at 0.6–1.25 μM H3K4me3. The yield of nicked intermediates was also stimulated by addition of H3K4me3 (Figure 1G, bottom); because these intermediates are obligatory, irreversible precursors of hairpins we deduce that H3K4me3 stimulates nicking. A reciprocal coupled cleavage assay using radiolabeled 23-RSS substrate and an unlabeled 12-RSS partner showed similar stimulation by H3K4me3 (Figures S2C and S2D). Thus, soluble H3K4me3 robustly stimulates DNA cleavage by RAG that has been depleted of endogenous H3K4me3.

RAG-2(388/405A$_{18}$) Exhibits Increased Basal Activity but Remains Responsive to H3K4me3

The ability of the 388/405A$_{18}$ mutation to rescue activity of a PHD finger mutant was consistent with (1) disruption of an autoinhibitory domain whose action in the wild-type protein is relieved by H3K4me3 or (2) disruption of a separate mode of autoinhibition whose action is independent of H3K4me3 binding. To test these possibilities, we assayed wild-type RAG-2, RAG-2(W453A), RAG-2(388/405A$_{18}$), and RAG-2(388/405A$_{18}$, W453A) (Figure 1E) for responsiveness to H3K4me3 in a coupled cleavage assay.

Equivalent amounts of active RAG tetramer, as determined by burst kinetic analysis (Figure S3), were assayed for coupled cleavage of a radiolabeled 12-RSS in the presence of increasing concentrations of H3K4me0 or H3K4me3 (Figure 2A). As expected, H3K4me3 stimulated hairpin formation by wild-type RAG: at 4 μM H3K4me3, the yield of hairpin product was more than 10-fold greater than in the absence of peptide (Figure 2B, right). Stimulation was specific, as H3K4me0 had no effect (Figure 2B, left). RAG-2(W453A) exhibited basal activity similar to that of wild-type (Figure 2B, left), but was unresponsive to H3K4me3 (Figure 2B, right), indicating that an intact PHD finger is required for stimulation. Consistent with its ability to rescue the recombination activity of RAG-2(W453A) in vivo, the 388/405A$_{18}$ mutation was associated with increased basal cleavage activity, either alone or in combination with W453A (Figure 2B, left). Despite this increase in basal activity, RAG-2(388/405A$_{18}$) was stimulable by H3K4me3 (Figure 2B); responsiveness required an intact PHD finger, as RAG-2(388/405A$_{18}$, W453A) was not stimulated (Figure 2B, right). Consistent with these observations, RAG-2 fragments bearing the W453A and the 388/405A$_{18}$, W453A double mutation failed to bind H3K4me3, whereas a fragment bearing the 388/405A$_{18}$ mutation retained the ability to bind (Figures S4A and S4B). Altogether, these observations indicate that (1) the 388/405A$_{18}$ gain-of-function mutation confers increased basal cleavage activity in vitro, but (2) this mutation provides partial relief of autoinhibition, sparing one or more additional inhibitory functions that can be relieved by H3K4me3 binding.

Tetramers composed of full-length RAG-1 and full-length RAG-2 are largely insoluble. For this reason quantitative studies of RAG activity have generally employed the more soluble truncated forms of RAG-1, RAG-2, or both. Nonetheless, we were able to purify sufficient full-length protein to determine that full-length RAG-1 (flR1-MH; Figure 1D), in complex with RAG-2(388/405A$_{18}$) or RAG-2(388/405A$_{18}$, W453A), exhibits increased basal nicking activity relative to a complex with RAG-2(W453A) (Figure S4C). Moreover, full-length RAG-1, in complex with RAG-2(388/405A$_{18}$), is stimulable by H3K4me3 in a PHD-dependent manner (Figure S4C). The elevated basal activity of the 388/405A$_{18}$ mutant and its responsiveness to H3K4me3 are consistent with the results of Figure 2B.

Stimulatory Effect of H3K4me3 on Substrate Binding

The stimulatory effect of the 388/405A$_{18}$ mutation could result from increased affinity for substrate, increased catalytic activity, or both. To distinguish these possibilities, we assessed substrate binding and catalysis. To measure affinity for DNA substrate, a 12-RSS fragment was incubated with increasing concentrations of wild-type RAG in the presence of 4 μM H3K4me0 or H3K4me3 peptide. Incubation was carried out in the presence of Ca^{2+}, which supports the binding of RAG to substrate in the absence of DNA cleavage. The fraction of total substrate remaining in the unbound state was determined (Figure 3A) and expressed as a function of active RAG concentration (Figure 3C), as defined by burst kinetics under the assumption that the active unit is a heterotetramer of composition
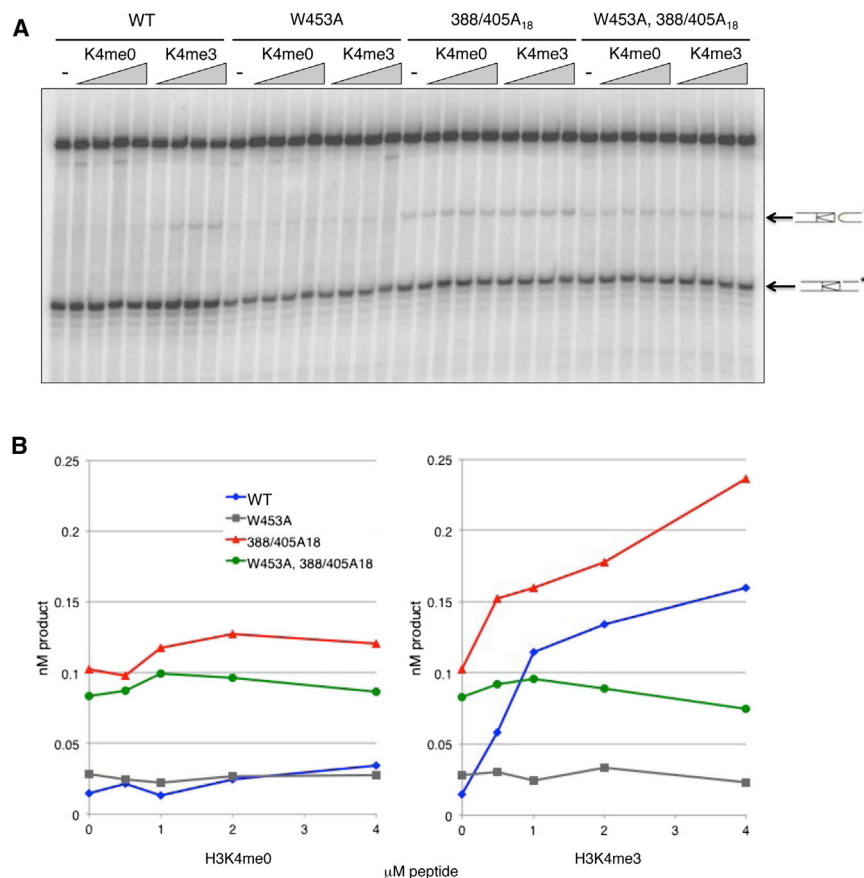
Figure 2. Mutation of the RAG-2 Autoinhibitory Domain Increases Coupled Cleavage Activity

(A) Coupled cleavage reactions contained radiolabeled 12-RSS, unlabeled 23-RSS, and wild-type (WT) RAG-2 or RAG-2 mutants as defined at top. K4me0 and K4me3, reactions supplemented with 0.5, 1, 2, or 4 μM H3K4me0 or H3K4me3 peptide; −, reactions lacking peptide. Positions of hairpin (HP) and nicked (N) products are indicated by arrows.

(B) Accumulation of hairpin product at 1 hr (nM product) is plotted as a function of the concentration of H3K4me0 (left) or H3K4me3 (right). Blue diamonds, wild-type RAG-2; gray squares, RAG-2(W453A); red triangles, RAG-2(388/405A$_{18}$); green circles, RAG-2(W453A, 388/405A$_{18}$).

Data in (A) and (B) are representative of more than three experiments.

(RAG-1)$_2$(RAG-2)$_2$ (Yu and Lieber, 2000). Dissociation constants, K$_D$, were determined (see the Experimental Procedures). The addition of H3K4me3 was accompanied by an increase in the affinity of wild-type RAG for substrate DNA, relative to control; in contrast, the affinity of RAG-2(388/405A$_{18}$) for a 12-RSS substrate was similar in the presence of H3K4me0 or H3K4me3 (Figures 3B and 3D). We also performed direct comparisons of substrate binding by each RAG species in the presence of H3K4me0 (Figure 3E) or H3K4me3 (Figure 3F). In the presence of control peptide, the affinities (K$_D$) of RAG-2(388/405A$_{18}$) and wild-type RAG for substrate were estimated at 88 nM and 242 nM, respectively (Figure 3G; Table S1). In the presence of H3K4me3, wild-type RAG and RAG-2(388/405A$_{18}$) bound substrate with an estimated K$_D$ of 76 nM and 84 nM, respectively (Figure 3H), similar to the affinity of RAG-2(388/405A$_{18}$) for substrate in the presence of H3K4me0. Thus the 388/405A$_{18}$ mutation confers a constitutive increase in substrate binding affinity by RAG independent of the presence of H3K4me3.

H3K4me3 and the RAG-2 388/405A$_{18}$ Mutation Stimulate Catalysis of DNA Cleavage

Because the 388/405A$_{18}$ mutation uncoupled the high affinity state from H3K4me3 binding, we were able to assess the effect of H3K4me3 on k$_{cat}$ in the absence of its effect on K$_D$. We assayed nicking of a 12-RSS substrate at concentrations of 10 nM to 60 nM by RAG-2(388/405A$_{18}$) in complex with cR1ct-MH. Reactions
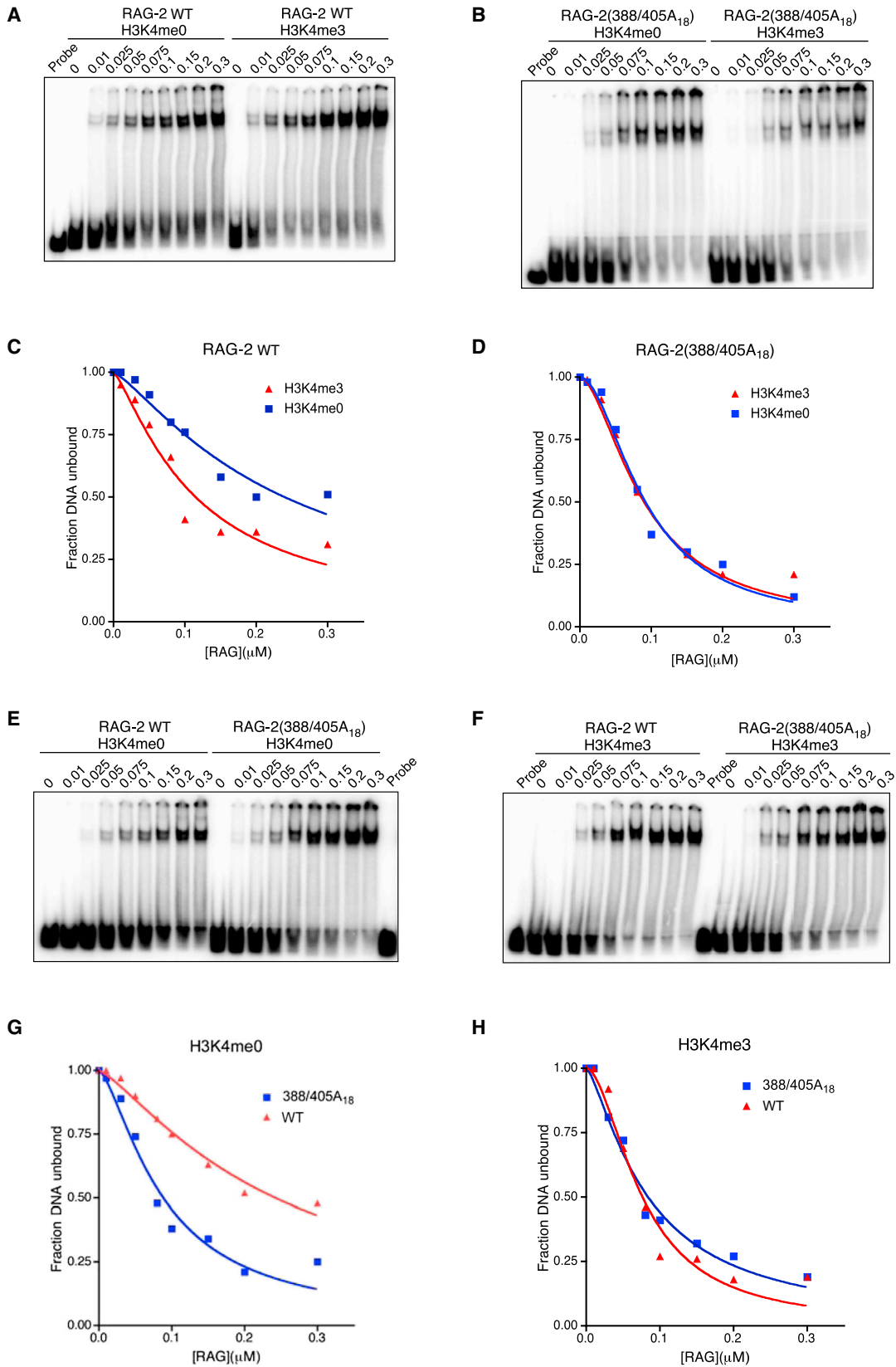
were carried out at an active RAG tetramer concentration of 1.5 nM in the presence of 4 μM H3K4me0 or H3K4me3 peptide (Figure 4A). Following determination of V$_{max}$ (Figures 4B and 4C), k$_{cat}$ was estimated (Experimental Procedures). In the presence of H3K4me0, RAG-2(388/405A$_{18}$) supported nicking with an apparent k$_{cat}$ of 4.95 min^{-1}, which increased to 7.06 min^{-1} in the presence of H3K4me3 (Figure 4C; Table S1). In comparison, we observed turnover rates of 0.83 min^{-1} and 3.76 min^{-1} for wild-type RAG-2 in the presence of H3K4me0 or H3K4me3, respectively (Figures S4D and S4E; Table S1), consistent with previous estimates (Shimazaki et al., 2009). Thus, the 388/405A$_{18}$ mutation is associated not only with increased affinity for substrate but also with a 6-fold increase in the basal k$_{cat}$ for DNA nicking; the basal k$_{cat}$ observed for RAG-2(388/405A$_{18}$) is similar to that observed for wild-type RAG-2 in the presence of H3K4me3. Nonetheless, RAG-2(388/405A$_{18}$) remains able to respond to H3K4me3 with an increase in catalytic rate. Taken together, these results are consistent with a model in which the RAG-2 autoinhibitory domain suppresses substrate binding and catalysis through separable effects that are overcome by binding of H3K4me3.

DISCUSSION

The accessibility of antigen receptor loci to RAG is associated with epigenetic modifications characteristic of active chromatin, such as H3K4me3, whose recognition by RAG-2 promotes V(D)J recombination. The ability of H3K4me3 to stimulate cleavage of naked DNA by RAG has suggested that H3K4me3 relieves autoinhibition exerted by some feature of the RAG complex.

One hint as to the nature of this autoinhibitory function was provided by the ability of the RAG-2 core to support V(D)J recombination despite its inability to bind H3K4me3. We now reconcile these properties by showing that the basal activity of
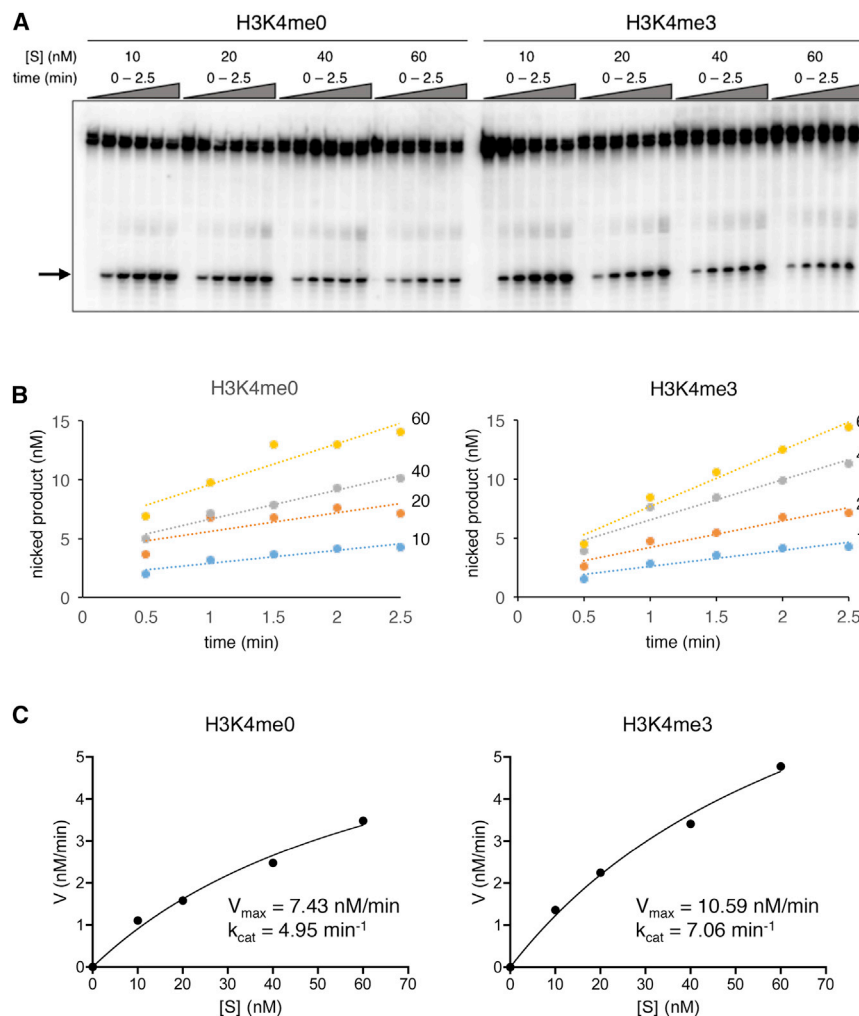
A RAG-2 WT H3K4me0 / RAG-2 WT H3K4me3

B RAG-2(388/405A$_{18}$) H3K4me0 / RAG-2(388/405A$_{18}$) H3K4me3

C RAG-2 WT

D RAG-2(388/405A$_{18}$)

E RAG-2 WT H3K4me0 / RAG-2(388/405A$_{18}$) H3K4me0

F RAG-2 WT H3K4me3 / RAG-2(388/405A$_{18}$) H3K4me3

G H3K4me0

H H3K4me3

(legend on next page)

Figure 4. Disruption of the RAG-2 Autoinhibitory Domain Mimics the Stimulatory Effect of H3K4me3 on Catalytic Rate

(A) Assay for RSS nicking. Reactions contained 1.5 nM RAG-2(388/405A$_{18}$) and 12-RSS substrate HL44/45 at 10, 20, 40, or 60 nM. Reactions were supplemented with 4 μM H3K4me0 or H3K4me3 peptide as indicated at top. Accumulation of nicked product (arrow) was assayed at times ranging from 0 to 2.5 min.

(B) Concentration of nicked product as determined in (A) is plotted against time for each substrate concentration. Blue, 10 nM; orange, 20 nM; gray, 40 nM; and yellow, 60 nM. Left: reactions containing H3K4me0; right: reactions containing H3K4me3.

(C) Reaction velocity (V) is plotted in nM/min as a function of substrate concentration ([S]). V$_{max}$ was determined by nonlinear regression analysis (Experimental Procedures); k$_{cat}$ = V$_{max}$/[RAG]$_T$, where [RAG]$_T$ is the total concentration of active RAG tetramer.

Data are representative of two experiments.

RAG is suppressed by an autoinhibitory domain that spans the boundary between the canonical core and noncore regions of RAG-2. Disruption of this autoinhibitory region uncouples V(D)J recombination from the requirement for H3K4me3 binding by RAG-2. Moreover, mutation of the autoinhibitory domain mimics the binding of H3K4me3 by increasing the affinity of RAG for substrate and enhancing its catalytic rate. Our observations support a model in which the responsiveness of RAG to epigenetic stimulation is conferred by an autoinhibitory domain whose action is relieved upon binding of H3K4me3.

The ability of exogenous H3K4me3 to stimulate the coupled cleavage activity of wild-type RAG was dependent, as expected, on binding of H3K4me3 to the PHD finger of RAG-2. When autoinhibition was relieved by the 388/405A$_{18}$ mutation, basal cleavage activity in the absence of H3K4me3 was similar to that observed for wild-type RAG in the presence of saturating H3K4me3 peptide. H3K4me3 binding exerts at least two effects that contribute to enhanced RSS cleavage activity in vitro: increased affinity of RAG for substrate and faster

---

Figure 3. The RAG-2 388/405A$_{18}$ Mutation Mimics the Stimulatory Effect of H3K4me3 on RAG-RSS Binding

(A) Electrophoretic mobility shift assay (EMSA) for binding of wild-type RAG to a consensus 12-RSS in the presence of H3K4me0 or H3K4me3 peptide as indicated at top. Probe, 12 RSS incubated in the absence of RAG. The concentration, in μM, of active RAG in each binding reaction is indicated above the lane.

(B) EMSA as in (A) except that RAG-2(388/405A$_{18}$) was substituted for wild-type RAG-2.

(C) H3K4me3 reduces the K$_D$ of RAG-RSS binding. The fraction of free probe (fraction DNA unbound) in each binding reaction of (A) was plotted as a function of active RAG concentration. Data from reactions containing H3K4me0 and H3K4me3 are indicated by blue squares and red triangles, respectively.

(D) The RAG-2 388/405A$_{18}$ mutation relieves responsiveness of RAG-RSS binding to H3K4me3. The fraction of free probe (fraction DNA unbound) in each binding reaction of (B) is plotted as in (C).

(E) EMSA for binding of wild-type RAG (left) or RAG-2(388/405A$_{18}$) (right) to a consensus 12-RSS in the presence of H3K4me0. Probe, 12 RSS incubated in the absence of RAG. The concentration of active RAG in each reaction is indicated above the lane.

(F) EMSA as in (E), except that H3K4me3 was substituted for H3K4me0.

(G) The RAG-2 388/405A$_{18}$ mutation increases basal affinity of RAG for RSS in the absence of H3K4me3. The fraction of free probe (fraction DNA unbound) in each binding reaction of (E) was plotted as a function of active RAG concentration. Data from reactions containing RAG-2(388/405A$_{18}$) and wild-type RAG-2 are indicated by blue squares and red triangles, respectively. K$_D$ estimates for wild-type (WT) and mutant (mut) proteins are indicated.

(H) The fraction of free probe (fraction DNA unbound) in each binding reaction of (F) is plotted as in (G).

Data in (A), (B), (E), and (F) are representative of three experiments.

catalysis. If the autoinhibitory domain confers allosteric activation by H3K4me3, then disruption of this domain would mimic the effects of H3K4me3 on substrate binding and catalysis. Indeed, the apparent K_D and k_{cat} for RAG-2(388/405A$_{18}$) in the absence of H3K4me3 were similar to those of wild-type RAG-2 in the presence of saturating H3K4me3. These observations indicate the presence of a functional element between residues 370 and 405 of RAG-2 that suppresses substrate binding and catalysis in the absence of H3K4me3. Our results are consistent with a model in which this autoinhibitory element maintains RAG in a state of low affinity for the RSSs until nearby transcriptional activation promotes allosteric activation through the deposition of H3K4me3.

The basal catalytic rate supported by RAG-2(388/405A$_{18}$) is similar to the maximally induced rate observed for wild-type RAG but is further increased in response to H3K4me3. While RAG-2(388/405A$_{18}$) supports a basal affinity for substrate that is also similar to the maximal induced affinity of wild-type RAG, H3K4me3 induces no further increase in affinity. Thus, the effects of H3K4me3 on substrate affinity and catalysis are separable. We imagine several possible reasons that the 388/405A$_{18}$ mutant may remain responsive to H3K4me3 with respect to catalytic rate. First, because the boundaries of the autoinhibitory domain, as defined genetically, extend beyond the limits of the 388/405A$_{18}$ mutation, RAG-2(388/405A$_{18}$) may retain residual autoinhibitory activity. Second, there may exist additional suppressive elements within the RAG complex that dampen the catalytic rate for DNA cleavage in the absence of H3K4me3. Third, the 388/405A$_{18}$ mutation may exert a gain-of-function effect separate from or in addition to its ability to mimic H3K4me3 binding. In any event, the 388/405A$_{18}$ mutation permits RAG to bypass recognition of H3K4me3 in vivo and mimics the stimulatory effects of H3K4me3 on substrate binding and turnover rate in vitro.

Available data do not provide structural insight into autoinhibition or its relief by H3K4me3. One model would invoke direct competition between the inhibitory domain and H3K4me3 for binding to the PHD finger. This seems unlikely, because the W453A mutation, which disrupts the H3K4me3 binding site, fails to relieve inhibition. Our results remain consistent with the possibility that the inhibitory domain exerts its suppressive effect through interactions with one or more regions of RAG distinct from the PHD finger. In this view, engagement of the PHD finger by H3K4me3 would relieve inhibition indirectly, perhaps through propagation of a conformational alteration within RAG.

The boundaries of the autoinhibitory domain lie within an acidic region of RAG-2, comprising residues 350 through 410. Neutralization of charge in this interval is associated with aberrant repair of RAG-mediated DNA breaks, decreased stability of RAG-signal end complexes (SECs), and genomic instability (Coussens et al., 2013). While these effects appear to reflect events occurring after RSS recognition and DNA cleavage, they may be explained in part by our results. An increase in genomic instability, for example, would be consistent with the uncoupling of substrate recognition and cleavage from H3K4me3 binding that we observe upon mutation of this region. A unifying hypothesis would suggest that the destabilization of SECs and relaxation of repair pathway choice are consequences of the structural

alterations that uncouple RAG activity from H3K4me3 binding upon mutation of the autoinhibitory domain. For example, if formation of a stable SEC were to require disengagement of RAG from H3K4me3, then mutations that mimic the effect of H3K4me3 engagement, such as RAG-2 388/405A$_{18}$, could compromise SEC stability and appropriate repair of DNA ends.

EXPERIMENTAL PROCEDURES

Cell Culture
NIH 3T3 and HEK293T cells were propagated in Dulbecco's modified Eagle's medium supplemented with 10% fetal bovine serum. Cells were maintained at 37°C in 5% CO_2.

Antibodies
Antibodies against the following proteins were used in this study: histone H3K4me3 (Millipore CMA-304), MBP (Santa Cruz Biotechnology sc-808), actin (Santa Cruz, sc-8432), and c-myc (Millipore CBL-430).

Oligonucleotide Substrates
Two pairs of duplex oligonucleotides were used in RSS cleavage and binding assays: DAR39/40 (12-RSS) and DAR61/62 (23-RSS) (McBlane et al., 1995) or HL44/45 (12-RSS) and HL46/47 (23-RSS) (Shimazaki et al., 2012). Oligonucleotides were purified by gel electrophoresis and 5′ end-labeled where indicated with ^{32}P by T4 DNA polynucleotide kinase (New England Biolabs). Complementary oligonucleotides were annealed as described previously (Lu et al., 2008).

DNA Binding Assays
Varying amounts of RAG tetramer up to 0.3 μM were combined with 1 nM radiolabeled HL44/45 in binding buffer (25 mM 3-(4-morpholino)propane sulfonic acid-KOH [pH 7.0], 30 mM KCl, 30 mM potassium glutamate, 6% glycerol, 0.1 mg/ml BSA, 4 mM CaCl$_2$, 1 mM dithiothreitol [DTT]) at a reaction volume of 10 μl. After 20 min at 37°C, 4 μl of 50% glycerol was added and reactions were resolved on a composite 4%/8% nondenaturing gel as described previously (Zhao et al., 2009). Radiolabeled species were detected on a phosphorimager, and the percent of total radioactivity present as free substrate at each RAG concentration was determined using ImageQuantNL (GE Healthcare). To determine the dissociation constant, K_D, data were fitted by nonlinear regression to the equation

$$F = \frac{K_D^n}{K_D^n + [RAG]^n},$$

where F is the fraction of substrate that is unbound, K_D is the dissociation constant, and n is the Hill coefficient. Nonlinear regression analysis was performed using GraphPad Prism v. 5.0 (GraphPad Software).

Determination of Catalytic Rate Constants
Wild-type or mutant RAG complexes (1.5 nM active tetramer, as determined by burst kinetic analysis) were combined with HL44/45 (at concentrations varying from 10 nM to 60 nM) in a buffer containing 25 mM 3-(4-morpholino)propane sulfonic acid-KOH (pH 7.0), 30 mM KCl, 30 mM potassium glutamate, 5 mM MgCl$_2$, 1 mM DTT, 1% glycerol, and 0.1 mg/ml BSA in reaction volumes of 20 μl at 37°C. Aliquots (2 μl) were withdrawn at varying times up to 3 min and reactions were stopped by addition of 1 vol 90% formamide/Tris-borate EDTA. Products were quantified as above. V_{max} was estimated by curve fitting to a Michaelis-Menton model (GraphPad Prism v. 5.0, GraphPad Software), and k_{cat} was determined from the relationship:

$$k_{cat} = \frac{V_{max}}{[RAG]_T}.$$

Expression constructs, protein purification, recombination assays, burst kinetic analysis, assays for coupled cleavage, and surface plasmon resonance are described in the Supplemental Experimental Procedures.

SUPPLEMENTAL INFORMATION

AUTHOR CONTRIBUTIONS

C.L., A.W., and J.B. conceived of, designed, and performed experiments. C.L., A.W., and J.B. drafted portions of the manuscript and edited the paper. S.D. conceived of experiments, designed experiments, interpreted results, and assumed primary responsibility for writing the manuscript.

ACKNOWLEDGMENTS

REFERENCES

Akamatsu, Y., Monroe, R., Dudley, D.D., Elkin, S.K., Gartner, F., Talukder, S.R., Takahama, Y., Alt, F.W., Bassing, C.H., and Oettinger, M.A. (2003). Deletion of the RAG2 C terminus leads to impaired lymphoid development in mice. Proc. Natl. Acad. Sci. USA *100*, 1209–1214.

Alt, F.W., Yancopoulos, G.D., Blackwell, T.K., Wood, C., Thomas, E., Boss, M., Coffman, R., Rosenberg, N., Tonegawa, S., and Baltimore, D. (1984). Ordered rearrangement of immunoglobulin heavy chain variable region segments. EMBO J. *3*, 1209–1219.

Callebaut, I., and Mornon, J.P. (1998). The V(D)J recombination activating protein RAG2 consists of a six-bladed propeller and a PHD fingerlike domain, as revealed by sequence analysis. Cell. Mol. Life Sci. *54*, 880–891.

Chakraborty, T., Chowdhury, D., Keyes, A., Jani, A., Subrahmanyam, R., Ivanova, I., and Sen, R. (2007). Repeat organization and epigenetic regulation of the DH-Cmu domain of the immunoglobulin heavy-chain gene locus. Mol. Cell *27*, 842–850.

Coussens, M.A., Wendland, R.L., Deriano, L., Lindsay, C.R., Arnal, S.M., and Roth, D.B. (2013). RAG2's acidic hinge restricts repair-pathway choice and promotes genomic stability. Cell Reports *4*, 870–878.

Cuomo, C.A., and Oettinger, M.A. (1994). Analysis of regions of RAG-2 important for V(D)J recombination. Nucleic Acids Res. *22*, 1810–1814.

Gellert, M. (2002). V(D)J recombination: RAG proteins, repair factors, and regulation. Annu. Rev. Biochem. *71*, 101–132.

Goldmit, M., Ji, Y., Skok, J., Roldan, E., Jung, S., Cedar, H., and Bergman, Y. (2005). Epigenetic ontogeny of the Igk locus during B cell development. Nat. Immunol. *6*, 198–203.

Grundy, G.J., Yang, W., and Gellert, M. (2010). Autoinhibition of DNA cleavage mediated by RAG1 and RAG2 is overcome by an epigenetic signal in V(D)J recombination. Proc. Natl. Acad. Sci. USA *107*, 22487–22492.

Hesse, J.E., Lieber, M.R., Gellert, M., and Mizuuchi, K. (1987). Extrachromosomal DNA substrates in pre-B cells undergo inversion or deletion at immunoglobulin V-(D)-J joining signals. Cell *49*, 775–783.

Jiang, H., Chang, F.C., Ross, A.E., Lee, J., Nakayama, K., Nakayama, K., and Desiderio, S. (2005). Ubiquitylation of RAG-2 by Skp2-SCF links destruction of the V(D)J recombinase to the cell cycle. Mol. Cell *18*, 699–709.

Jung, D., Giallourakis, C., Mostoslavsky, R., and Alt, F.W. (2006). Mechanism and control of V(D)J recombination at the immunoglobulin heavy chain locus. Annu. Rev. Immunol. *24*, 541–570.

Kirch, S.A., Rathbun, G.A., and Oettinger, M.A. (1998). Dual role of RAG2 in V(D)J recombination: catalysis and regulation of ordered Ig gene assembly. EMBO J. *17*, 4881–4886.

Lee, J., and Desiderio, S. (1999). Cyclin A/CDK2 regulates V(D)J recombination by coordinating RAG-2 accumulation and DNA repair. Immunity *11*, 771–781.

Li, Z., Dordai, D.I., Lee, J., and Desiderio, S. (1996). A conserved degradation signal regulates RAG-2 accumulation during cell division and links V(D)J recombination to the cell cycle. Immunity *5*, 575–589.

Liang, H.E., Hsu, L.Y., Cado, D., Cowell, L.G., Kelsoe, G., and Schlissel, M.S. (2002). The "dispensable" portion of RAG2 is necessary for efficient V-to-DJ rearrangement during B and T cell development. Immunity *17*, 639–651.

Liu, Y., Subrahmanyam, R., Chakraborty, T., Sen, R., and Desiderio, S. (2007). A plant homeodomain in RAG-2 that binds Hypermethylated lysine 4 of histone H3 is necessary for efficient antigen-receptor-gene rearrangement. Immunity *27*, 561–571.

Lu, H., Shimazaki, N., Raval, P., Gu, J., Watanabe, G., Schwarz, K., Swanson, P.C., and Lieber, M.R. (2008). A biochemically defined system for coding joint formation in V(D)J recombination. Mol. Cell *31*, 485–497.

Matthews, A.G., Kuo, A.J., Ramón-Maiques, S., Han, S., Champagne, K.S., Ivanov, D., Gallardo, M., Carney, D., Cheung, P., Ciccone, D.N., et al. (2007). RAG2 PHD finger couples histone H3 lysine 4 trimethylation with V(D)J recombination. Nature *450*, 1106–1110.

McBlane, J.F., van Gent, D.C., Ramsden, D.A., Romeo, C., Cuomo, C.A., Gellert, M., and Oettinger, M.A. (1995). Cleavage at a V(D)J recombination signal requires only RAG1 and RAG2 proteins and occurs in two steps. Cell *83*, 387–395.

Morshead, K.B., Ciccone, D.N., Taverna, S.D., Allis, C.D., and Oettinger, M.A. (2003). Antigen receptor loci poised for V(D)J rearrangement are broadly associated with BRG1 and flanked by peaks of histone H3 dimethylated at lysine 4. Proc. Natl. Acad. Sci. USA *100*, 11577–11582.

Ramón-Maiques, S., Kuo, A.J., Carney, D., Matthews, A.G., Oettinger, M.A., Gozani, O., and Yang, W. (2007). The plant homeodomain finger of RAG2 recognizes histone H3 methylated at both lysine-4 and arginine-2. Proc. Natl. Acad. Sci. USA *104*, 18993–18998.

Raval, P., Kriatchko, A.N., Kumar, S., and Swanson, P.C. (2008). Evidence for Ku70/Ku80 association with full-length RAG1. Nucleic Acids Res. *36*, 2060–2072.

Ross, A.E., Vuica, M., and Desiderio, S. (2003). Overlapping signals for protein degradation and nuclear localization define a role for intrinsic RAG-2 nuclear uptake in dividing cells. Mol. Cell. Biol. *23*, 5308–5319.

Sadofsky, M.J., Hesse, J.E., and Gellert, M. (1994). Definition of a core region of RAG-2 that is functional in V(D)J recombination. Nucleic Acids Res. *22*, 1805–1809.

Schatz, D.G., and Swanson, P.C. (2011). V(D)J recombination: mechanisms of initiation. Annu. Rev. Genet. *45*, 167–202.

Sekiguchi, J.A., Whitlow, S., and Alt, F.W. (2001). Increased accumulation of hybrid V(D)J joins in cells expressing truncated versus full-length RAGs. Mol. Cell *8*, 1383–1390.

Shimazaki, N., Tsai, A.G., and Lieber, M.R. (2009). H3K4me3 stimulates the V(D)J RAG complex for both nicking and hairpinning in trans in addition to tethering incis: implications for translocations. Mol. Cell *34*, 535–544.

Shimazaki, N., Askary, A., Swanson, P.C., and Lieber, M.R. (2012). Mechanistic basis for RAG discrimination between recombination sites and the off-target sites of human lymphomas. Mol. Cell. Biol. *32*, 365–375.

Steen, S.B., Han, J.O., Mundy, C., Oettinger, M.A., and Roth, D.B. (1999). Roles of the "dispensable" portions of RAG-1 and RAG-2 in V(D)J recombination. Mol. Cell. Biol. *19*, 3010–3017.

Subrahmanyam, R., Du, H., Ivanova, I., Chakraborty, T., Ji, Y., Zhang, Y., Alt, F.W., Schatz, D.G., and Sen, R. (2012). Localized epigenetic changes induced by DH recombination restricts recombinase to DJH junctions. Nat. Immunol. *13*, 1205–1212.

Talukder, S.R., Dudley, D.D., Alt, F.W., Takahama, Y., and Akamatsu, Y. (2004). Increased frequency of aberrant V(D)J recombination products in core RAG-expressing mice. Nucleic Acids Res. *32*, 4539–4549.

Yu, K., and Lieber, M.R. (2000). The nicking step in V(D)J recombination is independent of synapsis: implications for the immune repertoire. Mol. Cell. Biol. *20*, 7914–7921.

Zhang, L., Reynolds, T.L., Shan, X., and Desiderio, S. (2011). Coupling of V(D)J recombination to the cell cycle suppresses genomic instability and lymphoid tumorigenesis. Immunity *34*, 163–174.

Zhao, S., Gwyn, L.M., De, P., and Rodgers, K.K. (2009). A non-sequence-specific DNA binding mode of RAG1 is inhibited by RAG2. J. Mol. Biol. *387*, 744–758.